C Journal of Carbon Research

MDPI

Article

Activated Carbon from Stipa Tenacissima for the Adsorption of Atenolol

Nesrine Madani [1], Imane Moulefera [2,*], Souad Boumad [1], Diego Cazorla-Amorós [3], Francisco José Varela Gandía [3], Ouiza Cherifi [4] and Naima Bouchenafa-Saib [1]

[1] Laboratoire de Chimie Physique des Interfaces des Matériaux Appliqués à l'Environnement, Faculté de Technologie, Université Blida 1, B.P. 270 Route de Soumaa, Blida 09000, Algeria
[2] Chemical Engineering Department, Campus Universitario de Espinardo, University of Murcia, 30100 Murcia, Spain
[3] Dept. Química Inorgánica e Instituto Universitario de Materiales, Universidad de Alicante, Ap. 99, 03080 Alicante, Spain
[4] Laboratoire de Chimie du Gaz Naturel, Université des Science et de la Technologie Houarie Boumediene, Bab Ezzouar 16111, Algeria
* Correspondence: imane.moulefera@um.es

Abstract: The *Stipa tenacissima S*. is an endemic species of the Western Mediterranean countries, which grows on the semi-arid grounds of North Africa and South Spain. This biomass offers an abundant, renewable, and low-cost precursor for the production of activated carbon (AC). In that context, ACs were prepared by chemical activation of *Stipa tenacissima* leaves (STL) using phosphoric acid (H_3PO_4). The effects of activation temperature and impregnation ratio on the textural and chemical surface properties of the prepared activated carbons were investigated. Activation temperatures of 450 and 500 °C turned out to be the most suitable to produce activated carbons with well-developed porous textures. The best results in terms of developed surface area (1503 m^2/g) and micropore volume (0.59 cm^3/g) were observed for an STLs to phosphoric acid ratio of 1:2 and a carbonization temperature of 450 °C. The adsorption capacity of the optimal activated carbon was found to be 110 mg/g for the atenolol drug. The adsorption equilibrium was well explained by the pseudo-second-order model and Langmuir isotherm. This study showed that the chemical activation method using H_3PO_4 as an activating agent was suitable for developing STL-based activated carbon prepared for the removal of atenolol drug in an aqueous solution and compared with commercial activated carbon supplied by Darco.

Keywords: activated carbon; *Stipa tenacissima*; chemical activation; adsorption; atenolol

Citation: Madani, N.; Moulefera, I.; Boumad, S.; Cazorla-Amorós, D.; Gandía, F.J.V.; Cherifi, O.; Bouchenafa-Saib, N. Activated Carbon from Stipa Tenacissima for the Adsorption of Atenolol. *C* **2022**, *8*, 66. https://doi.org/10.3390/c8040066

Academic Editors: Indra Pulidindi, Pankaj Sharma and Aharon Gedanken

Received: 28 October 2022
Accepted: 19 November 2022
Published: 22 November 2022

1. Introduction

The rise in environmental concerns and pollution issues in recent years has prompted the search for new and sustainable green sources for the production of environmentally friendly materials for environmental applications. The use of biomass as precursors for the production of carbon materials received important attention from many researchers since this is a widely available and abundant source compared to traditional petroleum-based materials, which are polluting, toxic and non-biodegradable [1,2]. Currently, increasing focus is being paid to plant biomass as a raw material, and many industrial companies are following this trend with a major interest in developing economic bio-based products and materials from these renewable materials. Thus, the valorization of biomass into activated carbon is the subject of various works [3–7]. The global activated carbon market is expected to garner 2776 kilotons and 5129 million USD by 2022, registering a compound annual growth rate of 6.83% and 9.32% during the forecast period 2016–2020 [8]. The extensive use of activated carbon is mainly due to its large number of industrial

applications, including water and wastewater treatment [9–11], wastewater reclamation [12], gas purification [13–15], or as adsorbents for either CO_2 capture or high-pressure CH_4 storage [16,17] and also as catalysts [18–20] and catalyst supports [21,22]. Among the large variety of activation processes, chemical activation with phosphoric acid of biomass is one of the most employed methods for the preparation of activated carbon with enhanced physico-chemical properties [23,24]. It presents multiple advantages being the phosphoric acid not toxic compared to other impregnating chemicals [25], the low activating temperature required [25], a high yield obtained [26], and a well-developed mesoporosity [27]. Many factors, during preparation, play an important role in obtaining high-quality activated carbon. The knowledge and control of those variable factors during the activation process is very important in developing the porous texture of the activated carbon that is sought for given applications [9], as this last depends strongly on both, the activation process [16,28] and the nature of the precursor [29–31]. Hence, the influence of the preparation condition parameters such as impregnation ratios and activation temperature was deeply analyzed by many researchers [32,33].

Although there are many applications of activated carbon in different industries, adsorption still remains an effective process that results in extensive use of activated carbons. Consequently, the production of activated carbons with specific pore size distributions from low-cost materials at moderate temperatures is an important challenge on both, economical and energetical aspects [24]. Nowadays, ACs can be produced from a wide range of natural and synthetic substances and lignocellulosic materials being this last one the most used precursors [34–36]. The important content of cellulose and lignin in lignocellulosic materials has promoted them to be the most desired precursors for the preparation of activated carbon, being those two indispensables for getting a high carbon yield [37,38].

Removal of emergent pollutants from wastewater by different methods has been an important challenge for recent society and the subject of several studies over the last years [39–41]. Among them, pharmaceutical products have been widely reported due to their harmful effects on the environment such as paracetamols, clofenac, and some β-blocker species [42–44]. Atenolol is a beta blocker medicament usually used to treat high blood pressure or hypertension, heart rhythm problems, and angina [45]. Around 50% of the dose is not fully metabolized by the human body and is disposed of unchanged through urine [46]. Therefore, it has been extensively detected in concentrations ranging from about 0.78 μg/L to 6.6 μg/L in wastewater and hospital sewage [46,47].

In our previous study [48], the preparation of activated carbons from Stipa tenacissima leaves (STLs), a lignocellulosic plant widely abundant in Southern Algeria, through chemical activation with H_3PO_4 has been reported. It has been shown that relatively low temperatures are preferred for the preparation of activated carbons. For this purpose and with the attempt to obtain a well-developed porous texture at low temperatures, this study, on one hand, investigated the preparation of activated carbons from STLs by chemical activation with H_3PO_4 at different impregnation ratios (R) and activation temperatures (T). These factors were extensively examined. The study range varied from 400 to 600 °C and from 1 to 3 for both activation temperature and impregnation ratio, respectively. To check further the quality of our obtained ACs, atenolol medicament removal was used as a test to verify the adsorption capacities of three activated carbons, compared with commercial activated carbon from Darco (commercial DARCO G60 derived from lignin delivered by Fluka Chemika (ref. 05100), where the kinetics study was investigated and Freundlich and Langmuir models were reported as well.

2. Materials and Methods

2.1. Preparation of Activated Carbon

Washed clean STLs (collected from Southern Algeria) were dried in an oven at 110 °C for 24 h, which proved effective to facilitate subsequent crushing and grinding. The precursor was impregnated with an 85% H_3PO_4 solution at room temperature and dried for 2 h at 110 °C. The impregnation ratio, R, (H_3PO_4/precursor mass) (wt./wt.) was varied from 1 to 3. The samples were activated in a quartz reactor at different temperatures in the range of 400 to 600 °C under nitrogen flow at a rate of 100 mL/min and for 1 h as an activation time. The activated samples were cooled inside the furnace maintaining the N_2 flow. After that, the samples were washed with distilled water at 65 °C until neutral pH is achieved before being dried at 110 °C. The obtained activated carbons were named Rx-y, where R from ratio, while x and y correspond to the impregnation ratio and activation temperature, respectively.

2.2. Adsorption Equipment and Procedures

Atenolol ($C_{14}H_{22}N_2O_3$) (molecular weight: 266,336 g/mol, melting point: 147 °C, solubility of 13.3 mg/mL (at 25 °C), pKa1 = 9.6; pKa2 = 13.88, polar surface area 84.6 Å2 [49], solutions were prepared with distilled water at different initial concentrations. The equilibrium test was carried out inside glass flasks using 50 mg of dried activated carbon in contact with 100 mL of the atenolol solution at different initial concentrations in an orbital incubator (Gallenkamp, model INR-250) with an equivalent stirring rate of 200 rpm at 25 °C. The kinetic tests of atenolol adsorption were performed using a 100 mL atenolol solution with an initial concentration of 50 mg/L and 50 mg of activated carbon samples under continuous stirring for different time intervals. The concentration of atenolol was analyzed using double beam UV–visible spectrophotometer from Shimadzo (Series UV-1900) at a maximum absorption wavelength of 274 nm.

Adsorption capacity, for each equilibrium concentration, was calculated as is expressed in Equation (1):

$$q_e = \frac{C_0 - C_e}{w} \cdot V \quad (1)$$

where q_e is the equilibrium adsorption capacity (mg/g), C_0 and C_e are the initial and equilibrium concentrations, respectively, in mg/L; V is the solution volume (L) and W is the weight of the activated carbon (g).

The equilibrium adsorption data were fitted to the Langmuir, Freundlich, and Temkin adsorption isotherm models (Equation (2), (3) and (4), respectively).

$$q_e = \frac{q_L \,.\, K_L \,.\, \mathrm{C_e}}{1 + K_L.\mathrm{C_e}} \quad (2)$$

$$q_e = K_f.(C_e)^{1/n} \quad (3)$$

$$q_e = \frac{\mathrm{R}\,T}{K_1} \cdot \ln(K_2 \mathrm{C_e}) \quad (4)$$

where K_L is the equilibrium constant of Langmuir equation (L/mg), q_L is the maximum adsorption capacity (mg/g), K_f is the Freundlich constant associated to the adsorption capacity ((mg/g)(L/mg)$^{1/n}$) and n is the empirical parameter related to the energetic heterogeneity of the adsorption sites, where K_1 (J/mol) and k_2 (L/mg) is Temkin constant related to the heat of adsorption and isotherm constant, respectively [5].

The adsorption data were fitted to the first-order (Equation (5)), and second-order (Equation (6)) kinetic models for adsorption [48]:

$$Ln\,(q_\mathrm{e} - q_\mathrm{t}) = Ln(qe) - k_1 t \quad (5)$$

$$\frac{t}{q_t} = \frac{1}{k_2 \cdot {q_e}^2} + \frac{1}{q_e} t \quad (6)$$

where k_1 (L/min) and k_2 (g/mg·min) are the kinetic constants for the pseudo-first-order and second-order equation, respectively, and q_e is related to the adsorption capacity at equilibrium (mg/g).

2.3. Characterization

Thermal drying method is used for the determination of moisture content of the raw material. The STLs were dried at 110 °C until the consistency of weight was obtained. The moisture percentage in the sample was expressed as the loss in the mass due to drying as a percentage of the total mass of the sample.

Elemental analysis of the precursor and activated carbons was carried out in a CHNS Analyzer. Prior to analysis, the samples were dried overnight at 105 °C and cooled in desiccators. Oxygen content was obtained by the difference between the total percentage (100 wt.%) and the sum of percentages (wt.% dry ash-free) of nitrogen, carbon, hydrogen, and sulfur.

The textural properties of the prepared samples were assessed by nitrogen adsorption–desorption measurements at −196 °C using a Quantachrome Autosorb-6 apparatus. The materials were previously degassed at 250 °C for 4 h. The surface area (S_{BET}) was calculated from isotherms using the Brunauer–Emmett–Teller (BET) equation [50]. The volume of liquid nitrogen corresponding to the amount adsorbed at a relative pressure of $P/P_0 = 0.99$ was defined as total pore volume (V_T). The micropore volume ($V_{\mu p}$) was determined from Dubinin–Radushkevich equation [51].

3. Results and Discussion

3.1. Characterization

The results of the proximate analysis are compiled in Table 1. It can be seen that Stipa Tenacissima leaves (STLs) contain 62.81% volatile matter, 24.50% fixed carbon, and 1.19% ash. This composition follows the general trend of a typical biomass composition [34,52–54]. The high volatile matter and low ash content of biomass resources make them good starting materials for preparing activated carbons [55].

Table 1. Proximate analysis of Stipa tenacissima leaves (STLs).

Proximate Analysis	Weight (%)
Ash	1.19
Fixed carbon	24.50
Volatile matter	62.81
Moisture	11.50

Table 2 summarizes the elemental composition of the precursor and activated carbons prepared from STLs at different activation temperatures and impregnation ratios. The elemental composition, H/C, and O/C atomic ratios results indicate remarkable chemical changes in the surface after the activation process, while no sulfur (S) traces were detected for all the samples.

Table 2. Elemental analysis of the precursor and activated carbons produced at different activation temperatures and impregnation ratios (wt.%).

Samples	N	C	H	O *	O/C × 10^2	H/C × 10^2
STLs	1.10	47.70	6.40	44.80	93.92	13.42
R1-400	2.50	76.50	2.40	18.60	24.31	3.14
R1-450	0.50	81.60	2.10	15.80	19.36	2.57

R1-500	0.50	82.60	1.90	15.00	18.16	2.30
R1-600	0.40	91.00	1.60	7.00	7.69	1.76
R2-400	2.30	76.20	2.00	19.50	25.59	2.62
R2-450	0.40	78.40	1.70	19.50	24.87	2.17
R2-500	0.40	79.10	1.40	19.10	24.15	1.77
R2-600	0.30	81.60	1.40	16.70	20.47	1.72
R3-400	1.50	70.30	1.80	26.40	37.55	2.56
R3-450	0.20	72.00	1.50	26.30	36.53	2.08
R3-500	0.20	75.20	1.30	23.30	30.98	1.73
R3-600	0.20	78.30	1.30	20.20	25.80	1.66

(*): by difference.

The results demonstrated that carbon is the major constituent of the obtained ACs confirming the carbonaceous nature of the materials [55]. An increase in the carbon content from 47.74 wt.% for raw STLs to more than 70 wt.% could be observed in all the activated carbons with increasing activation temperature. As for the impregnation ratio of 1, the carbon content in activated carbons increased from 76.46 to 91.04 wt.% with increasing temperatures from 400 to 600 °C, which could be attributed to the increasing release of volatile matter. On another hand, hydrogen and oxygen content highly decreased, respectively, from 2.43 to 1.57 wt.%, and 18.56 to 6.99 wt.%, mainly as a result of the cleavage and breakage of bonds within the ACs structure that occurs during the activation process [56]. Moreover, the progressive decrease in the H/C and O/C atomic fractions (see Figure 1) observed for the obtained activated carbons with the different activation conditions, is indicative of the carbonization and activation processes.

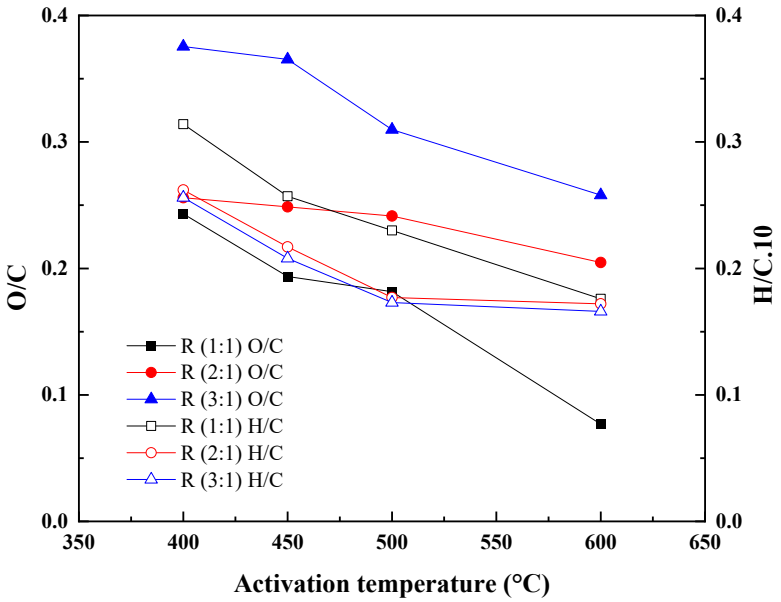

Figure 1. Effect of impregnation ratio and activation temperature on H/C and O/C fractions (H_3PO_4 concentration: wt. 85%; flow N_2 100 mL/min; activation duration: 1 h).

Indeed, during the activation process, polymeric structures decompose and liberate most of the non-carbon elements, mainly hydrogen, oxygen, and nitrogen in the form of liquid and gases, leaving behind a rigid carbon material with a short-range order [57,58].

Furthermore, as the impregnation ratio increases, carbon, and hydrogen contents decay, whereas the oxygen content increases from 15.53 wt.% for R1-500 to 34.80 wt.% for R3-500. This increase can be due to the progressive incorporation of phosphorus species with increasing the impregnation ratio.

Figure 2a,b, and c, respectively, show the N_2 adsorption–desorption isotherms at −196 °C of the prepared activated carbons from STLs with different impregnation ratios and at different activation temperatures. Figure 2a revealed that the isotherms of samples prepared with an impregnation ratio of (1:1) at different activation temperatures are of type I (b) based on IUPAC classification [59], showing a significant increase in the adsorption at low P/P_0 values, with barely defined knee, and long plateau which extends to $P/P_0 \approx 1.0$. This is indicative of the presence of large micropores and mesopores. In addition, an absence of hysteresis suggests that the obtained activated carbons contained mostly micropores with only a small contribution of mesopores.

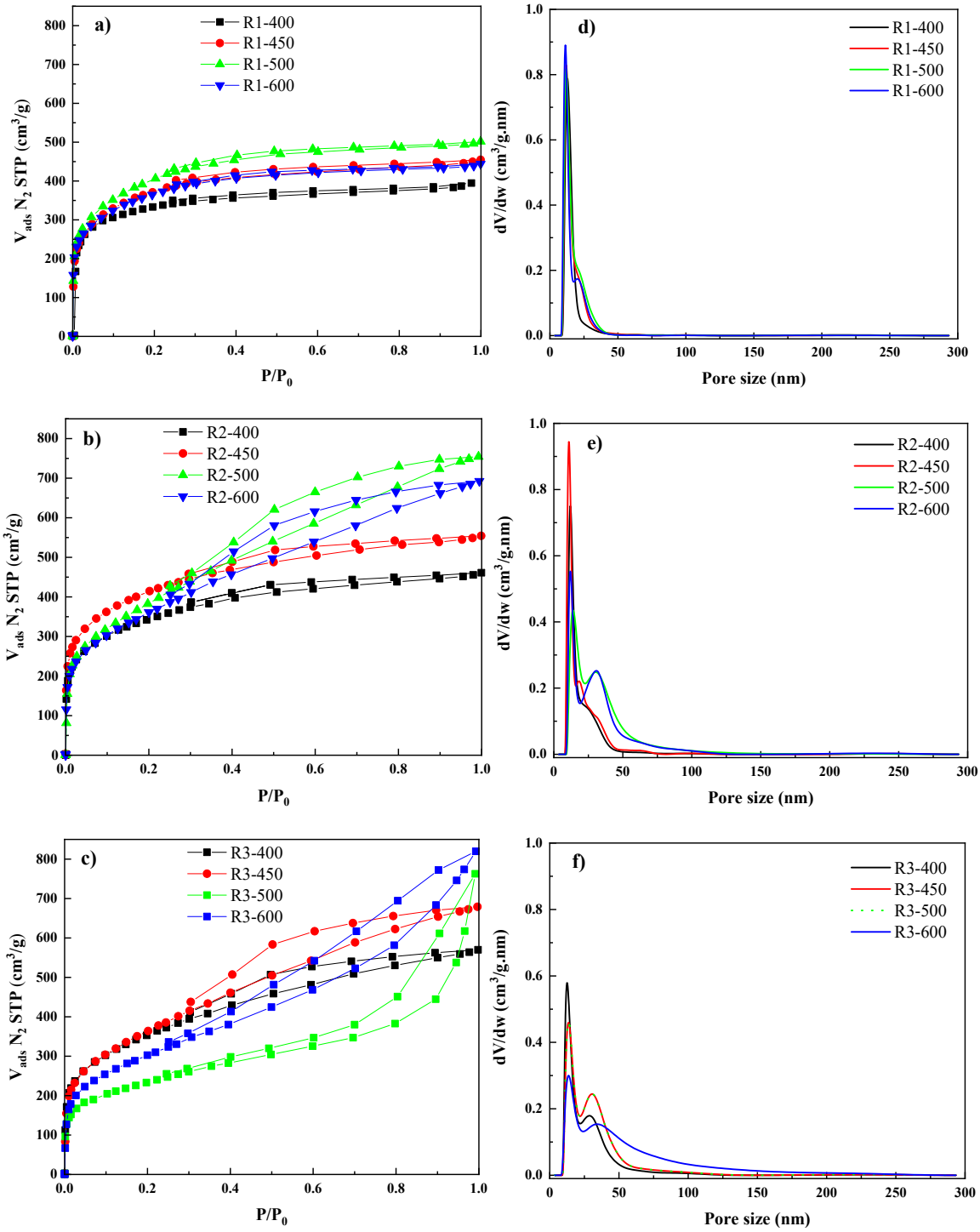

Figure 2. Adsorption–desorption isotherms of N_2 at −196 °C (**a**–**c**); and micropore size distribution (**d**–**f**) of activated carbons from STLs at different impregnation ratios and activation temperatures.

Figure 2b represents the adsorption isotherms of samples prepared with an impregnation ratio of (2:1) at different activation temperatures. The activated carbon obtained at 400 °C provides isotherm type I(b) which is typical of microporous materials where micropore filling may take place by primary filling at very low relative pressure. The activated carbons obtained at higher temperatures, exhibit a combination of type I and type IV(a) isotherms [59]. This indicates the presence of micro and mesoporosity leading to a gradual increase in adsorption after the initial filling of the micropores. The isotherms exhibit type H4 hysteresis, typical for slit-shaped pores.

For the impregnation ratio of (3:1) (Figure 2c) the activated carbons prepared at 400 °C exhibit type I (b) and the activated carbons prepared at 450, 500, and 600 °C a combination of type I and type IV (a) isotherms [59], with the presence of a hysteresis loop type H4. A small hysteresis in the shape was observed in the R3-400 and R3-450 samples. It means that the mesopores are developed during activation with an increasing of impregnation ratio to 3. Additionally, a larger hysteresis loop was observed for R3-500 which suggests a higher contribution of mesopores in their porosity.

The effect of activation temperature and impregnation ratio on the BET surface area, total pores volume, micropores, mesopores volume, and average pore diameter are given in Table 3. The optimum result in terms of surface area (1503 m^2/g) was obtained for an impregnation ratio of 2 as can be clearly seen in Table 4. The development of porosity goes through a maximum with the activation temperature, which is typically observed in phosphoric acid activation and is in agreement with our previous results [48]. It is known that phosphoric acid treatment accelerates structural alteration at low temperatures [60]. In fact, it has been reported [61] that at temperatures above 500 °C, the carbon structure shrinks, and the surface area decreases.

Table 3. Textural properties of the obtained activated carbons produced at different activation conditions.

Samples	S_{BET} (m^2/g)	V_{total} (cm^3/g)	$V_{\mu p}$ (cm^3/g)	V_{meso} (cm^3/g)	$V_{\mu p}/V_{tot}$	D_p (nm)
R1-400	1204	0.61	0.53	0.07	86.88	2.03
R1-450	1371	0.69	0.54	0.10	78.26	2.01
R1-500	1478	0.78	0.57	0.13	73.08	2.11
R1-600	1340	0.69	0.52	0.11	75.36	2.06
R2-400	1258	0.71	0.49	0.16	69.01	2.26
R2-450	1503	0.86	0.59	0.21	68.60	2.29
R2-500	1387	1.17	0.53	0.53	45.29	3.37
R2-600	1340	1.07	0.50	0.43	46.73	3.19
R3-400	1286	0.88	0.50	0.11	56.81	2.73
R3-450	1317	1.05	0.47	0.45	44.76	3.18
R3-500	1100	1.27	0.43	0.59	33.86	4.62
R3-600	838	1.18	0.33	0.33	27.97	5.63

S_{BET}: BET specific surface area; V_{Total}: total pore volume; $V_{\mu p}$: micropore volume; D_P: average pore diameter.

Girgis et al. have explained that the acid introduced into the material plays a double role [62]: (i) it produces hydrolysis of the lignocellulosic material with subsequent partial extraction of some components, thus weakening the particle which swells, and (ii) the acid occupies a volume which inhibits the contraction of the particle during the heat treatment, thus leaving a porosity when it is extracted by washing after carbonization [62].

Additionally, Jagtoyen et al. have reported that the phosphoric acid combines with organic species forming phosphate and polyphosphate bridges that connect biopolymer fragments and partially hindering the contraction in materials when the temperature

increases [63]. Above 450 °C, these bridges become thermally unstable, and their loss produces a contraction in the material, which will result in a decrease in porosity.

From this point of view, keeping the activation temperature at around 500 °C leads to better development of the adsorbent porosity. Several investigators have established that in the case of phosphoric acid activation of lignocellulosic material, temperatures neighboring 500 °C were suitable to obtain optimal properties of the activated carbons.

Impregnation ratio has been identified as one of the most important factors in the chemical activation process. With the increase in ratio from 1 to 3, the surface area and, mainly, total pore volumes also increased. The growth in porosity was attributed to the release of tars from the cross-linked framework generated by the treatment with phosphoric acid [64,65]. In fact, porosity is generated with phosphoric acid remaining in the internal structure of the biopolymer material in the form of phosphate and polyphosphate compounds. As the amount of H_3PO_4 used increases, the volume filled by it and various polyphosphates will increase, resulting in larger pore volume and pore size [57].

Figure 2d–f display the micropore size distribution of the different activated carbon obtained from the N_2 adsorption at −196 °C. As clearly observed the activated carbon with an impregnation ratio of 1 contain micropores in the range of 12–14 nm (Figure 2d). The increase in the impregnation ratios (Figure 2e,f) results in the appearance of a multimodal pore size distribution.

On the other hand, the experimental data in Table 3 also shows an increase in the percentage of mesoporosity with an increasing impregnation ratio, showing that the development of porosity is also accompanied by a widening of the porosity as the amount of H_3PO_4 is increased. These results support those extracted from the above-discussed pore size distribution. When the temperature exceeds 500 °C for the samples prepared with the impregnation ratio of (1:1) and 450 °C for the samples prepared with the impregnation ratio of (2:1) and (3:1), this trend is reversed. This change may be attributed to the increased merging and collapse of micropores which contributes to the reduction of surface area. J. Donald et al. have reported that the phosphate ester cross-links reach their limit of thermal stability at temperatures around 450–500 °C [66]. At higher temperatures, the breakdown of these cross-links would cause contraction and consequent reduction in porosity development.

3.2. Adsorption of Atenolol Drug

Three activated carbons were tested to check their removal efficiencies of a pharmaceutical drug "atenolol" from aqueous solution. A commercial activated carbon (CAC) was also used for comparison purposes. The equilibrium and kinetic studies of carbons were investigated. Table 4 contains the textual properties of the activated carbons used for the adsorption of atenolol.

Table 4. Textural properties of the tested activated carbons.

Samples	S_{BET} (m^2/g)	V_{total} (cm^3/g)	$V_{\mu p}$ (cm^3/g)	V_{meso} (cm^3/g)
R1-500	1478	0.78	0.57	0.13
R2-500	1387	1.17	0.53	0.53
R3-500	1100	1.27	0.43	0.59
CAC	909	0.76	0.36	0.40

3.2.1. Equilibrium Adsorption

The amounts of adsorbed atenolol (q_e) against the equilibrium concentration (Ce (mg/L)) at 25 °C are presented in Figure 3. The obtained isotherms are of type L and S for the prepared activated carbons and commercial activated carbon, respectively, according to Giles classification and commonly reported for adsorption in the liquid phase [67]. The L-shape isotherm showed a fairly rapid rise in adsorbed quantity as atenolol

concentration increases up to saturation which is characterized by a plateau. This indicates a progressive occupancy of the adsorbent surface as a function of concentration up until the entire surface area is coated with a single layer. Such adsorption behavior could be explained by the high affinity of adsorbent–adsorbate at low and moderate concentrations, which then decreases as concentration increases, since vacant adsorption sites decrease as the adsorbent becomes covered.

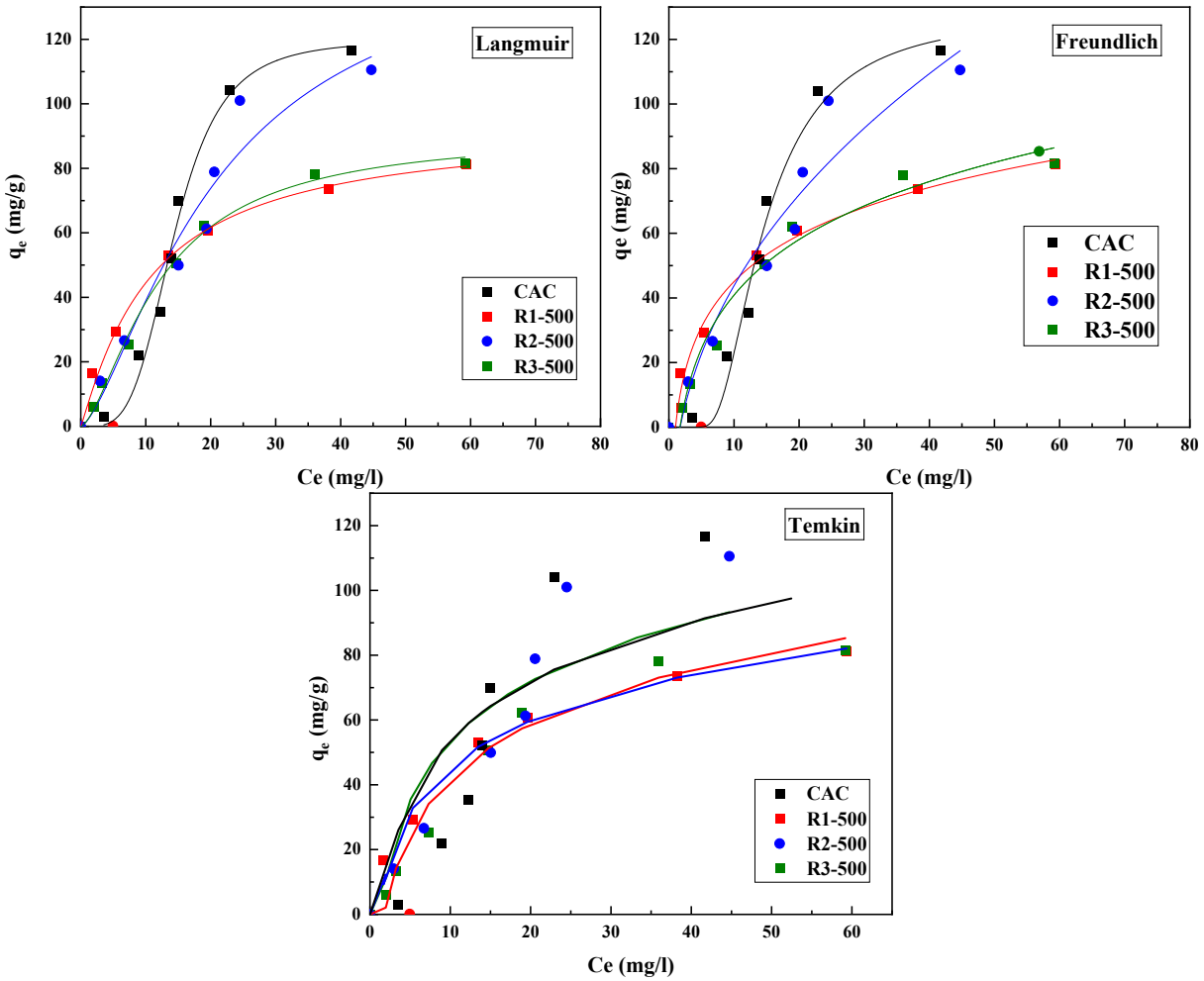

Figure 3. Adsorption isotherms of atenolol on the different activated carbons at 25 °C (symbols: experimental values; continuous lines: fitting to Langmuir, Freundlich and Temkin equations).

The S-shape isotherm showed a small sorption at low concentrations of atenolol in the solution and the sorption increased with the solute concentration. This type of isotherm indicates that at low concentrations the surface has a low affinity for the adsorbate, which increases at higher concentrations because of solute–solute attractive forces.

Furthermore, it can be observed that the adsorption capacity of the R1-500 and R3-500 presented the same amount of about 75 mg/g. However, R2-500 displays a higher adsorption capacity, above 110 mg/g and, with a similar adsorption capacity as for the CAC and this result is much higher compared to the literature [46]. This could mean that a high surface area of the adsorbents may not be the only parameter that determines the removal of higher amounts of the pollutant, but also the distribution of porosity could be a determining factor in this case [68]. This is confirmed by the porosity data (see Table 5), where the R2-500 presents a combination of both a high volume of micropores and an important mesoporous volume.

Three isotherms were used to fit the adsorption experimental results including Langmuir (Equation (2)), Freundlich (Equation (3)), and Temkin (Equation (4)) isotherms,

taking into account the effects of equilibrium concentration on adsorption capacity. The three model parameters and correlation coefficients (R^2) were listed in Table 5.

Table 5. Langmuir, Freundlich, and Temkin adsorption parameters obtained from equilibrium isotherms of atenolol for the activated carbons.

ACs	R1-500	R2-500	R3-500	CAC
Langmuir isotherm parameters				
q_L (mg/g)	98.65	169.69	115.69	126.52
K_L (L/mg)	0.08	0.04	0.05	0.06
R^2	0.99	0.95	0.99	0.99
Freundlich isotherm parameters				
K_F (m^2/g)	14.24	13.66	11.09	12.54
1/n	0.44	0.56	0.51	0.62
R^2	0.98	0.91	0.97	0.98
Temkin isotherm parameters				
K_1 (J/mol)	*121.06*	93.45	101.34	47.98
K_2 (L/mg)	*0.93*	0.75	0.55	0.23
R^2	*0.81*	0.81	0.83	0.87

It can be observed that in general terms, the highest R^2 values were obtained with the Langmuir model for all the tested carbons. The Langmuir adsorption isotherm describes the surface as homogeneous, assuming that there is no lateral interaction between adjacent adsorbed molecules when a single molecule occupies a single surface site. However, considering the shape of the CAC isotherm, this model is not found suitable and could not give the proper information to describe the adsorption process because it does not take into account adsorbate–adsorbate interactions. The maximum monolayer adsorption capacity predicted by the Langmuir model was 98.65, 169.69, and 115.69 mg/g for R1-500, R2-500, and R3-500, respectively.

The extent of the exponent, n, gives information on the favorability of adsorption. As deduced from the results, the values of 1/n were inferior to one (<1), meaning that the adsorption of atenolol was favorable on all samples. Furthermore, K_F is a rough index of the adsorption capacity. A high value of K_F indicates a high adsorption capacity, when the K_F value increases, the adsorption capacity of the adsorbent increases.

3.2.2. Kinetic Study

Figure 4 presents the adsorption kinetics of atenolol on studied carbons. It is clearly observed that the adsorption of AT was faster for samples R1-500 and CAC than that of R2-500 and R3-500 samples and the maximum uptake was reached in approximately 100 min. The quantity adsorbed at equilibrium found in this study (≈65 mg/g) appeared to be better than that reported by N.K Haro et al. (4.0 mg/g) [46].

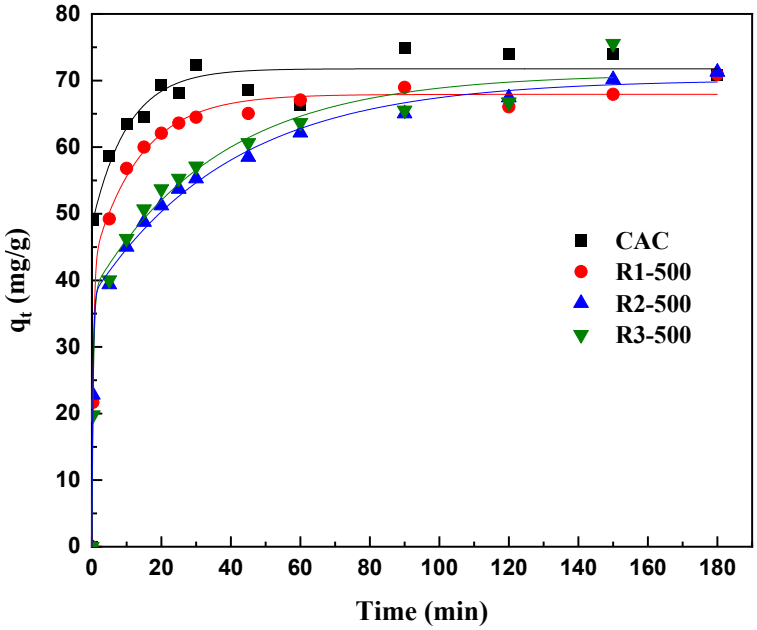

Figure 4. Adsorption kinetics of atenolol on different activated carbons at 25 °C, initial concentration C_0 = 50 mg/L; adsorbent concentration = 50 mg/L (experimental data: symbols; and second-order adsorption kinetic equation: continuous line).

Table 6 compiles the fitting parameters for the kinetic studies using (Equations (5) and (6)). The R^2 larger than 0.99 as well as the calculated q_{max} values close to the experimental ones indicated that atenolol uptake onto all adsorbents could be satisfactorily described by the pseudo-second-order model. This same tendency was observed in the adsorption of atenolol in a novel β-cyclodextrin adsorbent by Duan et al. [69] and the adsorption of atenolol in biocarbon designed from Melia Azedarach stones by Garcia et al. [70].

Table 6. Parameters obtained from kinetics curves of atenolol (C_0 = 50 mg/L; adsorbent concentration = 50 mg/L).

Acs	First-Order Model			Experiment	Second-Order Model		
	q_m (mg/g)	K.10² (L/mg)	R^2	q_{exp} (mg/g)	q_m (mg/g)	K.10² (L/mg)	R^2
R1-500	18.77	1.63	0.68	70.92	69.01	6.63	0.99
R2-500	36.51	2.12	0.94	71.27	69.75	2.16	0.99
R3-500	41.61	1.78	0.84	75.53	71.53	2.07	0.99
CAC	19.74	0.20	0.68	74.06	70.45	7.62	0.99

3.2.3. Mechanism of Atenolol Adsorption

The prepared activated carbon is negatively charged, and its surface is rich in oxygenated function. In addition, the pHpzc was found to be about 8. These facts allow the adsorption of atenolol being this last positively charged solution. The species of atenolol would be fixed on the surface of the activated carbon via the interaction H–H and H–O, and the secondary amine group of atenolol as shown in the following proposed mechanism (Figure 5).

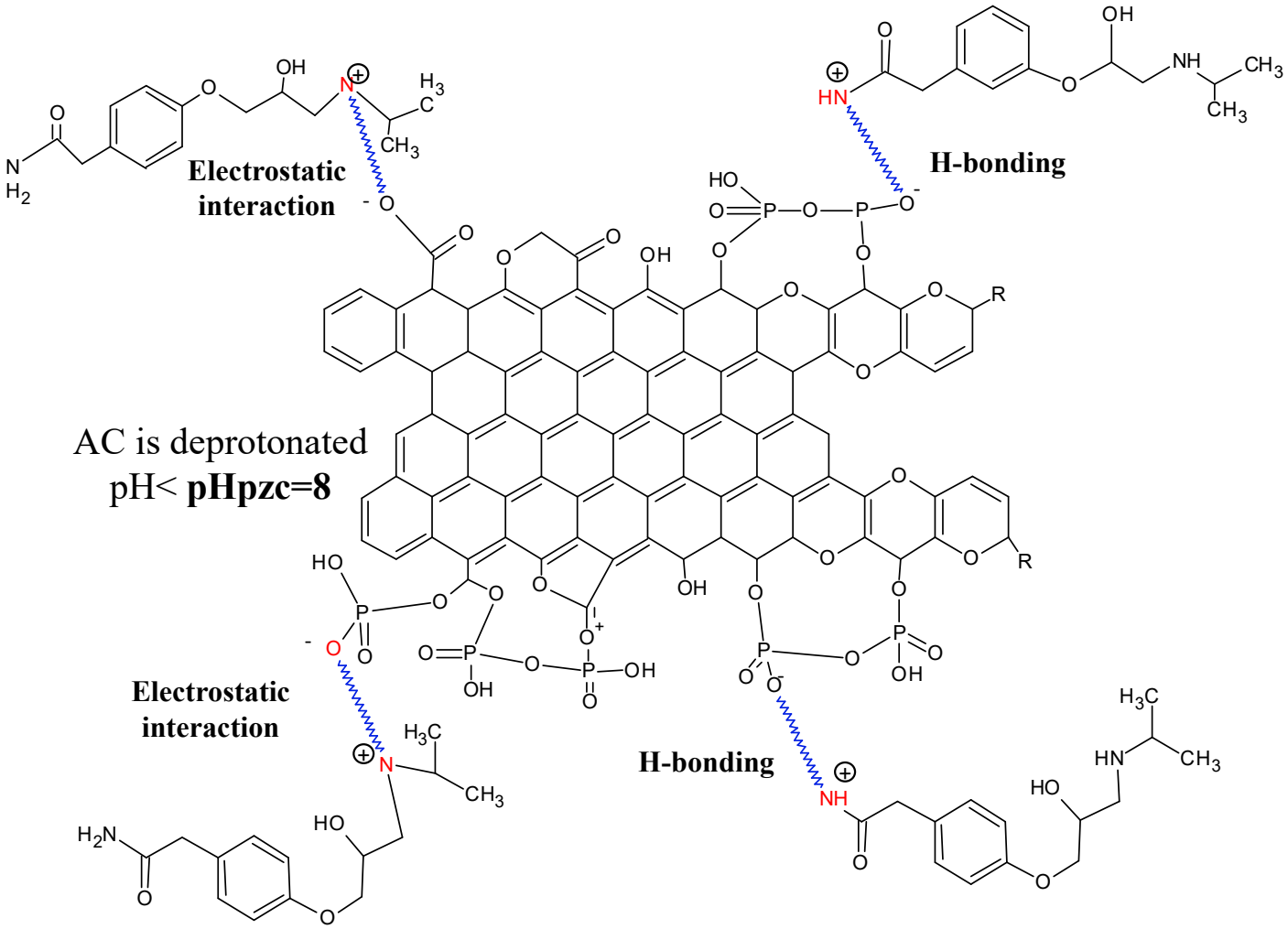

Figure 5. Adsorption mechanism of atenolol on activated carbon.

4. Conclusions

Activated carbons with a well-developed porosity were prepared from *Stipa tenacissima* leaves by chemical activation with phosphoric acid at different activation conditions. Generally, increasing the activating agent to STLs ratio from 1 to 3 increased the surface area and, especially, the total pore volume. The obtained results confirm that a 450 °C activation temperature and an impregnation ratio of 2 are suitable for obtaining an activated carbon with a surface area of 1503 m^2/g and pore volume of 0.59 cm^3/g. The synthesized activated carbons R1-500, R2-500, and R3-500 showed a good adsorption capacity for atenolol removal. The maximum adsorption capacities reached the value of 110 mg/g and showed a similar adsorption capacity as the commercial activated carbon from Darco. The equilibrium and adsorption kinetics results were satisfactorily fitted to Freundlich and Langmuir models and also to the second-order kinetic adsorption equation. Consequently, our findings suggest that a good quality activated carbon could be easily produced by one-step chemical activation with phosphoric acid from cheaper and sustainable raw materials such as *Stipa tenacisssima* leaves, and suitable for the elimination of pharmaceutical drugs and further environmental applications.

Author Contributions: N.M.: investigation, formal analysis, writing—original draft preparation; I.M.: methodology, writing—review and editing, formal analysis; S.B.: formal analysis, writing—review and editing; D.C.-A. and F.J.V.G.: formal analysis, reviewing and editing; N.B.-S. and O.C.: conceptualization, project administration, supervision, reviewing and editing. All authors discussed the results and commented on the manuscript. All authors have read and agreed to the published version of the manuscript.

Funding: This research received no external funding.

Institutional Review Board Statement: Not applicable.

Informed Consent Statement: Not applicable.

Acknowledgments: The authors thank the Ministry of Higher Education and Scientific Research of Algeria for the internship and the University of Alicante for their cooperation.

Conflicts of Interest: The authors declare no conflicts of interest.

References

1. Azwar, E.; Mahari, W.A.W.; Chuah, J.H.; Vo, D.-V.N.; Ma, N.L.; Lam, W.H.; Lam, S.S. Transformation of biomass into carbon nanofiber for supercapacitor application—A review. *Int. J. Hydrogen Energy* **2018**, *43*, 20811–20821. https://doi.org/10.1016/j.ijhydene.2018.09.111.
2. Moulefera, I.; Trabelsi, M.; Mamun, A.; Sabantina, L. Electrospun Carbon Nanofibers from Biomass and Biomass Blends—Current Trends. *Polymers* **2021**, *13*, 1071. https://doi.org/10.3390/polym13071071.
3. Nor, N.M.; Lau, L.C.; Lee, K.T.; Mohamed, A.R. Synthesis of activated carbon from lignocellulosic biomass and its applications in air pollution control—A review. *J. Environ. Chem. Eng.* **2013**, *1*, 658–666. https://doi.org/10.1016/j.jece.2013.09.017.
4. Vargas, A.M.; Cazetta, A.L.; Garcia, C.A.; Moraes, J.C.; Nogami, E.M.; Lenzi, E.; Costa, W.F.; Almeida, V.C. Preparation and characterization of activated carbon from a new raw lignocellulosic material: Flamboyant (Delonix regia) pods. *J. Environ. Manag.* **2011**, *92*, 178–184. https://doi.org/10.1016/j.jenvman.2010.09.013.
5. Zhong, Z.-Y.; Yang, Q.; Li, X.-M.; Luo, K.; Liu, Y.; Zeng, G.-M. Preparation of peanut hull-based activated carbon by microwave-induced phosphoric acid activation and its application in Remazol Brilliant Blue R adsorption. *Ind. Crops Prod.* **2012**, *37*, 178–185. https://doi.org/10.1016/j.indcrop.2011.12.015.
6. Liou, T.-H. Development of mesoporous structure and high adsorption capacity of biomass-based activated carbon by phosphoric acid and zinc chloride activation. *Chem. Eng. J.* **2010**, *158*, 129–142. https://doi.org/10.1016/j.cej.2009.12.016.
7. Yahya, M.A.; Al-Qodah, Z.; Zanariah Ngah, C.W. Agricultural bio-waste materials as potential sustainable precursors used for activated carbon production: A review. *Renew. Sustain. Energy Rev.* **2015**, *46*, 218–235. https://doi.org/10.1016/j.rser.2015.02.051.
8. Allied Market Research. Activated Carbon Market by Product Type (Powdered, Granular), Application (Liquid, Gaseous) and End Use (Water Treatment, Food & Beverage Processing, Air purification)—Global Opportunity Analysis and Industry Forecast, 2014–202. *Allied Mark. Res*. 2022. Available online: https://www.alliedmarketresearch.com/activated-carbon-market (accessed on 4 August 2022).
9. Acharya, J.; Sahu, J.N.; Mohanty, C.; Meikap, B. Removal of lead(II) from wastewater by activated carbon developed from Tamarind wood by zinc chloride activation. *Chem. Eng. J.* **2009**, *149*, 249–262. https://doi.org/10.1016/j.cej.2008.10.029.
10. Tsai, W.-T.; Lai, C.-W.; Su, T.-Y. Adsorption of bisphenol-A from aqueous solution onto minerals and carbon adsorbents. *J. Hazard. Mater.* **2006**, *134*, 169–175. https://doi.org/10.1016/j.jhazmat.2005.10.055.
11. García-Mateos, F.; Ruiz-Rosas, R.; Marqués, M.; Cotoruelo, L.; Rodríguez-Mirasol, J.; Cordero, T. Removal of paracetamol on biomass-derived activated carbon: Modeling the fixed bed breakthrough curves using batch adsorption experiments. *Chem. Eng. J.* **2015**, *279*, 18–30. https://doi.org/10.1016/j.cej.2015.04.144.
12. Kalkan, .; Yapsakli, K.; Mertoglu, B.; Tufan, D.; Saatci, A. Evaluation of Biological Activated Carbon (BAC) process in wastewater treatment secondary effluent for reclamation purposes. *Desalination* **2011**, *265*, 266–273. https://doi.org/10.1016/j.desal.2010.07.060.
13. Guo, J.; Xu, W.S.; Chen, Y.L.; Lua, A.C. Adsorption of NH3 onto activated carbon prepared from palm shells impregnated with H_2SO_4. *J. Colloid Interface Sci.* **2004**, *281*, 285–290. https://doi.org/10.1016/j.jcis.2004.08.101.
14. Sun, Y.; Yang, G.; Zhang, J.; Wang, Y.; Yao, M. Activated Carbon Preparation from Lignin by H3PO4 Activation and Its Application to Gas Separation. *Chem. Eng. Technol.* **2011**, *35*, 309–316. https://doi.org/10.1002/ceat.201100309.
15. Dolores, L.-C.; Juan, P.M.-L.; Falco, C.; Titirici, M.-M.; Diego, C.-A. Diego, Porous Biomass-Derived Carbons: Activated Carbons. In *Sustainable Carbon Materials from Hydrothermal Processes*; John Wiley & Sons, Ltd.: Hoboken, NJ, USA, 2013; pp. 75–100. https://doi.org/10.1002/9781118622179.ch3.
16. Calvo-Muñoz, E.M.; García-Mateos, F.J.; Rosas, J.; Rodríguez-Mirasol, J.; Cordero, T. Biomass Waste Carbon Materials as adsorbents for CO2 Capture under Post-Combustion Conditions. *Front. Mater.* **2016**, *3*, 1–14. https://doi.org/10.3389/fmats.2016.00023.
17. Ozdemir, S.; Ozdemir, S.; Yetilmezsoy, K. Poultry abattoir sludge as bio-nutrient source for walnut plantation in low-fertility soil. *Environ. Prog. Sustain. Energy* **2019**, *38*, e13066. https://doi.org/10.1002/ep.

18. García-Mateos, F.J.; Moulefera, I.; Rosas, J.M.; Benyoucef, A.; Rodríguez-Mirasol, J.; Cordero, T. Alcohol Dehydrogenation on Kraft Lignin-Derived Chars with Surface Basicity. *Catalysts* **2017**, *7*, 308. https://doi.org/10.3390/catal7100308.
19. Matos, I.; Bernardo, M.; Fonseca, I. Porous carbon: A versatile material for catalysis. *Catal. Today* **2017**, *285*, 194–203. https://doi.org/10.1016/j.cattod.2017.01.039.
20. Zhang, S.; Yin, H.; Wang, J.; Zhu, S.; Xiong, Y. Catalytic cracking of biomass tar using Ni nanoparticles embedded carbon nanofiber/porous carbon catalysts. *Energy* **2020**, *216*, 119285. https://doi.org/10.1016/j.energy.2020.119285.
21. Szymański, G.; Rychlicki, G. Catalytic conversion of propan-2-ol on carbon catalysts. *Carbon* **1993**, *31*, 247–257. https://doi.org/10.1016/0008-6223(93)90028-9.
22. Arampatzidou, A.C.; Deliyanni, E.A. Comparison of activation media and pyrolysis temperature for activated carbons development by pyrolysis of potato peels for effective adsorption of endocrine disruptor bisphenol-A. *J. Colloid Interface Sci.* **2016**, *466*, 101–112. https://doi.org/10.1016/j.jcis.2015.12.003.
23. Moulefera, I.; García-Mateos, F.J.; Benyoucef, A.; Rosas, J.M.; Rodríguez-Mirasol, J.; Cordero, T. Effect of Co-solution of Carbon Precursor and Activating Agent on the Textural Properties of Highly Porous Activated Carbon Obtained by Chemical Activation of Lignin with H_3PO_4. *Front. Mater.* **2020**, *7*, 1–14. https://doi.org/10.3389/fmats.2020.00153.
24. Xu, J.; Chen, L.; Qu, H.; Jiao, Y.; Xie, J.; Xing, G. Preparation and characterization of activated carbon from reedy grass leaves by chemical activation with H_3PO_4. *Appl. Surf. Sci.* **2014**, *320*, 674–680. https://doi.org/10.1016/j.apsusc.2014.08.178.
25. Kan, Y.; Yue, Q.; Li, D.; Wu, Y.; Gao, B. Preparation and characterization of activated carbons from waste tea by H 3 PO 4 activation in different atmospheres for oxytetracycline removal. *J. Taiwan Inst. Chem. Eng.* **2017**, *71*, 494–500. https://doi.org/10.1016/j.jtice.2016.12.012.
26. Romero, A.; Lillo-Rodenas, M.A.; de Lecea, C.S.-M.; Linares-Solano, A. Hydrothermal and conventional H3PO4 activation of two natural bio-fibers. *Carbon* **2012**, *50*, 3158–3169. https://doi.org/10.1016/j.carbon.2011.10.031.
27. Bouchenafa-Saïb, N.; Mekarzia, A.; Bouzid, B.; Mohammedi, O.; Khelifa, A.; Benrachedi, K.; Belhaneche-Bensemra, N. Removal of malathion from polluted water by adsorption onto chemically activated carbons produced from coffee grounds. *Desalin. Water Treat.* **2013**, *52*, 4920–4927. https://doi.org/10.1080/19443994.2013.808845.
28. Marsh, H.; Rodríguez-Reinoso, F. Preface. In *Activated Carbon*; Marsh, H., Rodríguez-Reinoso, F., Eds.; Elsevier Science Ltd.: Oxford, UK, 2006; pp. xv–xvi. https://doi.org/10.1016/b978-008044463-5/50013-3.
29. Rodríguez-Reinoso, F.; Molina-Sabio, M. Textural and chemical characterization of microporous carbons. *Adv. Colloid Interface Sci.* **1998**, *76–77*, 271–294. https://doi.org/10.1016/s0001-8686(98)00049-9.
30. Nielsen, L.; Biggs, M.J.; Skinner, W.; Bandosz, T.J. The effects of activated carbon surface features on the reactive adsorption of carbamazepine and sulfamethoxazole. *Carbon* **2014**, *80*, 419–432. https://doi.org/10.1016/j.carbon.2014.08.081.
31. Zhang, J.P.; Sun, Y.; Woo, M.W.; Zhang, L.; Xu, K.Z. Preparation of steam activated carbon from black liquor by flue gas precipitation and its performance in hydrogen sulfide removal: Experimental and simulation works. *J. Taiwan Inst. Chem. Eng.* **2016**, *59*, 395–404. https://doi.org/10.1016/j.jtice.2015.09.005.
32. Vernersson, T.; Bonelli, P.R.; Cerrella, E.G.; Cukierman, A.L. *Arundo donax* cane as a precursor for activated carbons preparation by phosphoric acid activation. *Bioresour. Technol.* **2002**, *83*, 95–104. https://doi.org/10.1016/s0960-8524(01)00205-x.
33. Jagtoyen, M.; Groppo, J.; Derbyshire, F. Activated carbons from bituminous coals by reaction with H3PO4: The influence of coal cleaning. *Fuel Process. Technol.* **1993**, *34*, 85–96. https://doi.org/10.1016/0378-3820(93)90093-j.
34. Nabais, J.V.; Laginhas, C.; Carrott, M.R.; Carrott, P.; Amorós, J.C.; Gisbert, A.N. Surface and porous characterisation of activated carbons made from a novel biomass precursor, the esparto grass. *Appl. Surf. Sci.* **2013**, *265*, 919–924. https://doi.org/10.1016/j.apsusc.2012.11.164.
35. Fierro, V.; Torné-Fernández, V.; Celzard, A.; Montané, D. Influence of the demineralisation on the chemical activation of Kraft lignin with orthophosphoric acid. *J. Hazard. Mater.* **2007**, *149*, 126–133. https://doi.org/10.1016/j.jhazmat.2007.03.056.
36. Tancredi, N.; Cordero, T.; Mirasol, J.R.; Rodríguez, J.J. Activated carbons from Uruguayan eucalyptus wood. *Fuel* **1996**, *75*, 1701–1706. https://doi.org/10.1016/s0016-2361(96)00168-8.
37. Hernández, V. *Lignocellulosic Precursors Used in the Synthesis of Activated Carbon-Characterization Techniques and Applications in the Wastewater Treatment*; InTech: Houston, TX, USA, 2012. https://doi.org/10.5772/3346.
38. González-García, P. Activated carbon from lignocellulosics precursors: A review of the synthesis methods, characterization techniques and applications, Renew. Sustain. *Energy Rev.* **2018**, *82*, 1393–1414. https://doi.org/https://doi.org/10.1016/j.rser.2017.04.117.
39. Lin, Z.; Wang, D.; Zhang, H.; Li, L.; Huang, Z.; Shen, J.; Lin, Y. Extraction and determination of malachite green from aquatic products based on molecularly imprinted polymers. *Sep. Sci. Technol.* **2016**, *51*, 1684–1689. https://doi.org/10.1080/01496395.2016.1175478.
40. Das, A.K.; Saha, S.; Pal, A.; Maji, S.K. Surfactant-modified alumina: An efficient adsorbent for malachite green removal from water environment. *J. Environ. Sci. Health Part A* **2009**, *44*, 896–905. https://doi.org/10.1080/10934520902958708.
41. Farooqi, Z.H.; Sultana, H.; Begum, R.; Usman, M.; Ajmal, M.; Nisar, J.; Irfan, A.; Azam, M. Catalytic degradation of malachite green using a crosslinked colloidal polymeric system loaded with silver nanoparticles. *Int. J. Environ. Anal. Chem.* **2020**. https://doi.org/10.1080/03067319.2020.1779247.
42. Zaccariello, G.; Moretti, E.; Storaro, L.; Riello, P.; Canton, P.; Gombac, V.; Montini, T.; Rodríguez-Castellón, E.; Benedetti, A. TiO_2–mesoporous silica nanocomposites: Cooperative effect in the photocatalytic degradation of dyes and drugs. *RSC Adv.* **2014**, *4*, 37826–37837. https://doi.org/10.1039/c4ra06767c.

43. Al Qarni, H.; Collier, P.; O'Keeffe, J.; Akunna, J. Investigating the removal of some pharmaceutical compounds in hospital wastewater treatment plants operating in Saudi Arabia. *Environ. Sci. Pollut. Res.* **2016**, *23*, 13003–13014. https://doi.org/10.1007/s11356-016-6389-7.
44. Rezaei, R.; Aghapour, A.A.; Khorsandi, H. Investigating the biological degradation of the drug β-blocker atenolol from wastewater using the SBR. *Biogeochemistry* **2022**, *33*, 267–281. https://doi.org/10.1007/s10532-022-09979-w.
45. Marques, S.C.; Mestre, A.S.; Machuqueiro, M.; Gotvajn, A..; Marinšek, M.; Carvalho, A.P. Apple tree branches derived activated carbons for the removal of β-blocker atenolol. *Chem. Eng. J.* **2018**, *345*, 669–678. https://doi.org/10.1016/j.cej.2018.01.076.
46. Haro, N.K.; Del Vecchio, P.; Marcilio, N.R.; Feris, L. Removal of atenolol by adsorption—Study of kinetics and equilibrium. *J. Clean. Prod.* **2017**, *154*, 214–219. https://doi.org/10.1016/j.jclepro.2017.03.217.
47. Ahmad, A.A.; Din, A.T.M.; Yahaya, N.K.E.; Karim, J.; Ahmad, M.A. Atenolol sequestration using activated carbon derived from gasified Glyricidia sepium. *Arab. J. Chem.* **2020**, *13*, 7544–7557. https://doi.org/10.1016/j.arabjc.2020.08.029.
48. Madani, N.; Bouchenafa-Saib, N.; Mohammedi, O.; Varela-Gandía, F.; Cazorla-Amorós, D.; Hamada, B.; Cherifi, O. Removal of heavy metal ions by adsorption onto activated carbon prepared from Stipa tenacissima leaves. *Desalin. Water Treat.* **2017**, *64*, 179–188. https://doi.org/10.5004/dwt.2017.20254.
49. Miroslav, F.; Radka, K.; Oksana, G.; Zuzana, S.; Aleš, K.; Antonín, N.; Martin, K.; Roman, G. Sorption of atenolol, sulfamethoxazole and carbamazepine onto soil aggregates from the illuvial horizon of the Haplic Luvisol on loess. *Soil Water Res.* **2018**, *13*, 177–183. https://doi.org/10.17221/82/2018-swr.
50. Brunauer, S.; Emmett, P.H.; Teller, E. Adsorption of Gases in Multimolecular Layers. *J. Am. Chem. Soc.* **1938**, *60*, 309–319. https://doi.org/10.1021/ja01269a023.
51. Dubinin, M.M.; Zaverina, E.D.; Timofeyev, D.P. Sorption and structure of active carbons. I. Adsorption of organic vapors. *Zhurnal Fiz. Khimii* **1947**, *21*, 1352–1362.
52. Sayğılı, H.; Güzel, F.; Önal, Y. Conversion of grape industrial processing waste to activated carbon sorbent and its performance in cationic and anionic dyes adsorption. *J. Clean. Prod.* **2015**, *93*, 84–93. https://doi.org/10.1016/j.jclepro.2015.01.009.
53. Demiral, I.; Şamdan, C.A. Preparation and Characterisation of Activated Carbon from Pumpkin Seed Shell Using H_3PO_4. *Anadolu Univ. J. Sci. Technol. Appl. Sci. Eng.* **2016**, *17*, 125–138. https://doi.org/10.18038/btda.64281.
54. Tadda, M.A.; Ahsan, A.; Shitu, A.; ElSergany, M.; Arunkumar, T.; Jose, B.; Daud, N.N. A review on activated carbon: Process, application and prospects. *J. Adv. Civ. Eng. Pract. Res.* **2016**, *2*, 7–13.
55. Das, D.; Samal, D.P.; Bc, M. Preparation of Activated Carbon from Green Coconut Shell and its Characterization. *J. Biosens. Bioelectron.* **2015**, *6*, 100248. https://doi.org/10.4172/2157-7048.1000248.
56. Durán-Valle, C.J. Techniques Employed in the Physicochemical Characterization of Activated Carbons. In *Lignocellulosic Precursors Used in the Synthesis of Activated Carbon-Characterization Techniques and Applications in the Wastewater Treatment*; Montoya, V.H., Petriciolet, A.B., Eds.; IntechOpen: London, UK, 2012; pp. 38–58. Available online: https://books.google.dz/books?id=DnmszQEACAAJ (accessed on 4 August 2022).
57. Yakout, S.; El-Deen, G.S. Characterization of activated carbon prepared by phosphoric acid activation of olive stones. *Arab. J. Chem.* **2016**, *9*, S1155–S1162. https://doi.org/10.1016/j.arabjc.2011.12.002.
58. Angin, D. Production and characterization of activated carbon from sour cherry stones by zinc chloride. *Fuel* **2014**, *115*, 804–811. https://doi.org/10.1016/j.fuel.2013.04.060.
59. Thommes, M.; Kaneko, K.; Neimark, A.V.; Olivier, J.P.; Rodriguez-Reinoso, F.; Rouquerol, J.; Sing, K.S.W. Physisorption of gases, with special reference to the evaluation of surface area and pore size distribution (IUPAC Technical Report). *Pure Appl. Chem.* **2015**, *87*, 1051–1069. https://doi.org/10.1515/pac-2014-1117.
60. Jagtoyen, M.; Thwaites, M.; Stencel, J.; McEnaney, B.; Derbyshire, F. Adsorbent carbon synthesis from coals by phosphoric acid activation. *Carbon* **1992**, *30*, 1089–1096. https://doi.org/10.1016/0008-6223(92)90140-r.
61. Kriaa, A.; Hamdi, N.; Srasra, E. Removal of Cu (II) from water pollutant with Tunisian activated lignin prepared by phosphoric acid activation. *Desalination* **2010**, *250*, 179–187. https://doi.org/10.1016/j.desal.2008.12.056.
62. Girgis, B.S.; Yunis, S.S.; Soliman, A.M. Characteristics of activated carbon from peanut hulls in relation to conditions of preparation. *Mater. Lett.* **2002**, *57*, 164–172. https://doi.org/10.1016/s0167-577x(02)00724-3.
63. Jagtoyen, M.; Derbyshire, F. Activated carbons from yellow poplar and white oak by H3PO4 activation. *Carbon* **1998**, *36*, 1085–1097. https://doi.org/10.1016/s0008-6223(98)00082-7.
64. Prahas, D.; Kartika, Y.; Indraswati, N.; Ismadji, S. Activated carbon from jackfruit peel waste by H3PO4 chemical activation: Pore structure and surface chemistry characterization. *Chem. Eng. J.* **2008**, *140*, 32–42. https://doi.org/10.1016/j.cej.2007.08.032.
65. Jun, T.Y.; Latip, N.H.A.; Abdullah, A.M.; Latif, P.A. Effect of Activation Temperature and Heating Duration on Physical Characteristics of Activated Carbon Prepared from Agriculture Waste. *Environ. Asia* **2010**, *3*, 143–148.
66. Donald, J.; Ohtsuka, Y.; Xu, C. Effects of activation agents and intrinsic minerals on pore development in activated carbons derived from a Canadian peat. *Mater. Lett.* **2011**, *65*, 744–747. https://doi.org/10.1016/j.matlet.2010.11.049.
67. Giles, C.H.; Smith, D.; Huitson, A. A general treatment and classification of the solute adsorption isotherm. I. Theoretical. *J. Colloid Interface Sci.* **1974**, *47*, 755–765. https://doi.org/10.1016/0021-9797(74)90252-5.
68. Qu, W.; Yuan, T.; Yin, G.; Xu, S.; Zhang, Q.; Su, H. Effect of properties of activated carbon on malachite green adsorption. *Fuel* **2019**, *249*, 45–53. https://doi.org/10.1016/j.fuel.2019.03.058.
69. Duan, C.; Wang, J.; Liu, Q.; Zhou, Y.; Zhou, Y. Efficient removal of Salbutamol and Atenolol by an electronegative silanized β-cyclodextrin adsorbent. *Sep. Purif. Technol.* **2021**, *282*, 120013. https://doi.org/10.1016/j.seppur.2021.120013.

70. García-Rosero, H.; Romero-Cano, L.A.; Aguilar-Aguilar, A.; Bailón-García, E.; Carvalho, A.P.; Pérez-Cadenas, A.F.; Carrasco-Marín, F. Adsorption and thermal degradation of Atenolol using carbon materials: Towards an advanced and sustainable drinking water treatment. *J. Water Process. Eng.* **2022**, *49*, 102978. https://doi.org/10.1016/j.jwpe.2022.102987.